

Quantum phase transitions in alternating spin- $(\frac{1}{2}, \frac{5}{2})$ Heisenberg chains

Antônio S. F. Tenório, R. R. Montenegro-Filho, and M. D. Coutinho-Filho
*Laboratório de Física Teórica e Computacional, Departamento de Física,
 Universidade Federal de Pernambuco, CEP 50670-901, Recife, Pernambuco, Brazil*

The ground state spin-wave excitations and thermodynamic properties of two types of ferrimagnetic chains are investigated: the alternating spin-1/2 spin-5/2 chain and a similar chain with a spin-1/2 pendant attached to the spin-5/2 site. Results for magnetic susceptibility, magnetization and specific heat are obtained through the finite-temperature Lanczos method with the aim in describing available experimental data, as well as comparison with theoretical results from the semi-classical approximation and the low-temperature susceptibility expansion derived from Takahashi's modified spin-wave theory. In particular, we study in detail the temperature vs. magnetic field phase diagram of the spin-1/2 spin-5/2 chain, in which several low-temperature quantum phases are identified: the Luttinger Liquid phase, the ferrimagnetic plateau and the fully polarized one, and the respective quantum critical points and crossover lines.

PACS numbers: 75.10.Pq, 75.10.Jm, 75.30.Kz, 75.40.Mg

I. INTRODUCTION

Quasi-one-dimensional magnetic materials form a class of compounds with magnetic properties that above a characteristic temperature can be described through one-dimensional models [1]. These include systems with a rotationally invariant singlet ground state (GS), modeled, for example, through spin-1 gapped and gapless critical spin-1/2 chains [1], as well as more complex structures, such as ladders [1] and spin tubes [2]. Typically, gapless one-dimensional systems exhibit power-law decay of the correlation functions and can be understood through the Bethe ansatz [3] or the Luttinger Liquid theory [1]. In addition, in gapped one-dimensional (1D) systems the application of an external magnetic field B can suppress the gap and induce a quantum phase transition [4] to a Luttinger Liquid phase. In particular, an extensive study of the B - temperature (T) phase diagram of a spin-1/2 gapped ladder system was recently carried out [5, 6].

Contrary to the above mentioned systems, quasi-1D ferrimagnetic compounds display GS spontaneous magnetization and have ferromagnetic and antiferromagnetic (AF) spin-wave excitations. Usually the AF spin-wave mode is gapped and the magnetization curve exhibits a plateau, which can be explained by topological arguments [7]. Ferrimagnetism can arise from the topology of the unit cell [8], as in the phosphates with chemical formula $A_3Cu_3(PO_4)_4$, where $A = Ca, Sr$ or Pb . These materials have three Cu^{2+} spin-1/2 ions [9] and can be modeled by a line of spin-1/2 trimer clusters [10, 11] with AF exchange couplings. Another class of ferrimagnets are mixed-spin compounds of type $(A-X-B-X)_n$, where A and B are two different magnetic components (single ions or more complex molecules) and X is a bridging ligand. In particular, we are interested in compounds that can be modeled by spin-1/2 spin-5/2 chains (sS chains); this includes, for example, systems built from Mn^{2+} and Cu^{2+} ions linked through a dithioxalato ligand [12, 13]. Further, in the composition of some ferrimagnets, magnetic elements can be organic radicals like the nitronyl ni-

troxide free radicals (NITR), where R stands for an alkyl (methyl, ethyl) or aromatic group (phenyl). A family into this category consists of the Mn -NITR compounds [14], for which there is an AF exchange coupling between the spin-1/2 radicals and the spin-5/2 Mn^{2+} ions.

In this work we present a numerical study of the thermodynamic properties of the ferrimagnetic chains illustrated in Fig. 1: spin-1/2 spin-5/2 alternating chain (sS chain) and the spin-1/2 spin-5/2 alternating chain with a spin-1/2 pendant attached to the spin-5/2 site (ssS chain). These chains can be respectively used to model the ferrimagnetic compounds $CuMn(S_2C_2O_2)_2 \cdot 7.5H_2O$ (denoted by $CuMnDTO$) [13] and $[Mn(NITIm)(NITImH)]ClO_4$ (denoted by $MnNN$) [15], whose crystal structures belong to the centrosymmetric monoclinic space group $P2_1/c$ (C_{2h}). The 3D ordered phase observed [13, 15, 16] in these compounds, and in similar ones [17], at very low- T have been intensively investigated. In fact, magnetization measurements [15, 16] suggest that the canting of the ferrimagnetic moments of the chains give rise to a 3D weak ferromagnetism below the critical temperature, although neutron-diffraction experiments [17] in similar compounds indicate a canted AF structure. A common feature in these compounds is that the Mn^{2+} ion has a $^6S_{5/2}$ GS, thereby leading to a single ion anisotropy with no zero-field splitting in first order of perturbation theory. Very low- T magnetization measurements in a noncentrosymmetric orthorhombic compound [17], belonging to the space group $P2_12_12_1$, suggest a single-ion anisotropy $D/k_B \approx 40$ mK, which is much smaller than the intra-chain AF exchange couplings of the referred compounds [13, 15–17]. Therefore, a proper description of the 1D-3D magnetic transition may require, in general, anisotropic couplings, including the dipolar interaction. However, similarly to previous analysis [13, 15], in order to describe the 1D ferrimagnetic properties of the compounds, we disregard anisotropy effects.

The GS and the low-energy magnetic excitations are calculated through the Lanczos exact diagonalization

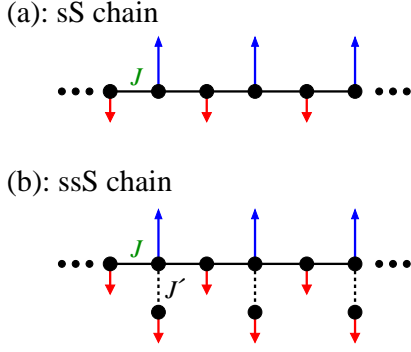


FIG. 1: (Color online) Schematic representation of the exchange couplings and the GS long-range ferrimagnetic ordering for the (a) sS and (b) ssS alternating chains.

(ED) algorithm, while thermal properties are obtained by the finite-temperature Lanczos method (FTLM) [18]. We also explore the field-induced quantum phase transitions of these systems and discuss our results in light of experimental data, as well as predictions from the semiclassical approximation [19] and the modified spin-wave (MSW) theory [3].

This work will unfold as follows: in Sec. II, we describe the theoretical models and methods employed. In Sec. III, we estimate the model parameters suitable to describe the experimental data (susceptibility and magnetization) of the related compounds. In Sec. IV, the one magnon bands and the specific heats of the two systems are presented and the main features discussed. In Sec. V we exhibit the $T - B$ phase diagram of the sS chain and discuss in detail its quantum critical points and crossover lines, the Luttinger liquid phase and the plateau regions. In Sec. VI, we analyze the low-temperature behavior of the zero-field magnetic susceptibility and, finally, in Sec. VII we present a discussion of our relevant findings.

II. MODELS AND METHODS

The sS chain with a uniform exchange interaction $J(> 0)$ and N_c [s,S] cells is described by the following Hamiltonian:

$$H_{sS} = J \sum_i^{N_c} (\mathbf{S}_i + \mathbf{S}_{i+1}) \cdot \mathbf{s}_i - g\mu_B B S^z, \quad (1)$$

where $s = 1/2$ and $S = 5/2$, the g -factor is assumed uniform, μ_B is the Bohr magneton, B is an applied magnetic field in the z direction and S^z is the operator for the z component of the total spin. This chain is bipartite, with N_c sites with spin- $5/2$ in one sublattice and N_c sites with spin- $1/2$ in the other; therefore, the Lieb and Mattis theorem [20] assures that the GS total spin, S_{GS} , is given by $N_c|S - s| = 2N_c$, i. e., spin 2 per unit cell. The GS magnetic ordering of this chain is sketched in Fig. 1(a).

The ssS chain with N_c [s,S,s'] cells is described by the following Hamiltonian:

$$H_{ssS} = J \sum_{l=1}^{N_c} \mathbf{s}_l \cdot (\mathbf{S}_l + \mathbf{S}_{l+1}) + J' \sum_{l=1}^{N_c} \mathbf{S}_l \cdot \mathbf{s}'_l - g\mu_B B S^z, \quad (2)$$

where $s = s' = 1/2$ and $S = 5/2$, while $J > 0$ and $J' > 0$. The Lieb and Mattis theorem assures that $S_{GS} = N_c|S - 2s| = 3N_c/2$, i. e., spin $\frac{3}{2}$ per unit cell. The GS magnetic order of this chain is sketched in Fig. 1(b).

The FTLM [18] is based on the Lanczos diagonalization technique and random sampling. The fundamental relations used in FTLM for the calculation of an static quantity associated to an operator A are

$$\begin{aligned} \langle A \rangle &\approx \frac{N_{st}}{ZR} \sum_{r=1}^R \sum_{j=0}^{\mathcal{M}} e^{-\beta \epsilon_j^r} \langle r | \psi_j^r \rangle \langle \psi_j^r | A | r \rangle, \\ Z &\approx \frac{N_{st}}{R} \sum_{r=1}^R \sum_{j=0}^{\mathcal{M}} e^{-\beta \epsilon_j^r} |\langle r | \psi_j^r \rangle|^2, \end{aligned} \quad (3)$$

where the sampling is carried over R random states $|r\rangle$, taken as initial states for a \mathcal{M} -step Lanczos procedure which results in \mathcal{M} approximate eigenvalues ϵ_j^r with respective eigenvectors $|\psi_j^r\rangle$ in the N_{st} -dimensional Hilbert space. The method allow us to calculate the temperature dependence of the magnetization per unit cell m_c , magnetic susceptibility per unit cell χ , and specific heat C through: $m_c = g\mu_B \frac{\langle S^z \rangle}{N_c}$, $\chi = g^2 \mu_B^2 \frac{\langle (S^z)^2 \rangle - \langle S^z \rangle^2}{N_c k_B T}$, and $C = \frac{\langle H^2 \rangle - \langle H \rangle^2}{k_B T^2}$, where k_B is the Boltzmann constant. The total number of sites $N = 2N_c$ for the sS chain and $N = 3N_c$ for the ssS chain. In the computation we have used periodic boundary conditions, $\mathcal{M} = 50$ for both chains and $R = 40000$ (50000) for the sS (ssS) chain. A full diagonalization study of the specific heat and susceptibility for the sS chain with $N_c = 3$ can be found in Ref. [21].

III. MAGNETIC SUSCEPTIBILITY AND MODEL PARAMETERS

Through a semiclassical approach, in which the S spins are treated as classical variables, Seiden [19] derived a closed formula for the magnetic susceptibility χ . In particular, the quantity $T\chi(T)$ has a minimum at a temperature T_{min} which is generally situated in a region where $\beta JS < 1$, a feature which has been known to be typical of 1D ferrimagnets. Similarly, a closed expression for the susceptibility of the ssS chain can also be established [15].

In Fig. 2(a) we present data for the magnetic susceptibility of the compound CuMnDTO (from Refs. [13, 19]) together with FTLM, with $J/k_B = 44.8$ K and $g = 1.90$, and semiclassical-approximation [19] results, with $J/k_B = 59.7$ K and $g = 1.9$, for the sS chain. For

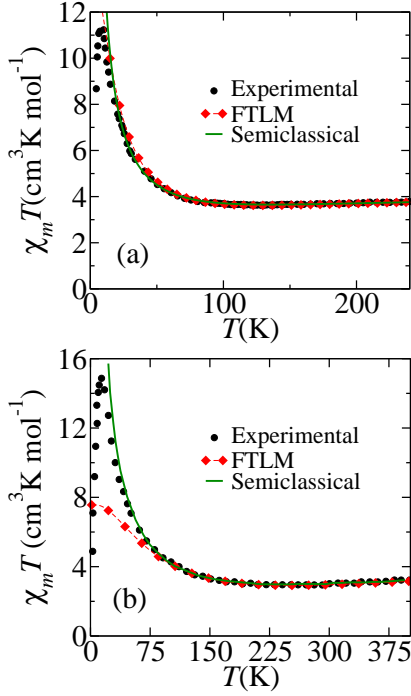


FIG. 2: (Color online) Molar susceptibility χ_m times temperature T of the (a) sS and (b) ssS chains as a function of T . Experimental: data of (a) the compound CuMnDTO from Ref. [13] and of (b) the MnNN compound from Ref. [15]. FTLM: (a) $N = 16$, $g = 1.90$ and $J = 44.8$ K, (b) $N = 18$, $g = 2.0$, $J/k_B = 150$ K and $J'/k_B = 255$ K. Semiclassical: (a) Ref. [19] (with $J/k_B = 59.7$ K, $S = 2.5$ and $g = 1.9$) and (b) Ref. [15] (with $J/k_B = 141$ K, $J'/k_B = 250$ K, $S = 2.5$ and $g = 2.0$).

the FTLM results, the estimation of J is made by using the value of the minimum of the experimental curve: $T_{min} = 130$ K. We see that both the FTLM and the semiclassical approach agree with the experimental data in the mid- and high-temperature regimes. As the temperature is lowered below T_{min} , χT increases and presents a maximum at $T_{max} = 7.5$ K, which marks the onset of the tridimensional ordering. For a strictly one-dimensional system it is expected, from the Mermin-Wagner theorem [22], that long-range order (LRO) may occur only at $T = 0$. We remark that for quantum ferromagnetic [23] chains the correlation length diverges as $1/T$ and the susceptibility as $1/T^2$; further, the low-lying magnetic excitations of ferrimagnetic chains present a ferromagnetic character (see below) and the same referred critical behavior is shown [24] to hold, which explains the increase in the curve of χT just below $T = T_{min}$.

In Fig. 2(b) we present FTLM and semiclassical results [15] for the ssS chain, and experimental data [15] of the MnNN compound. A profile similar to that of Fig. 2(a) is observed with $T_{min} = 255$ K. Taking $g = 2.0$, our estimative for the model parameters, J and J' , are $J' = 1.7J$, with $J/k_B = 150$ K and $J'/k_B = 255$ K. We also

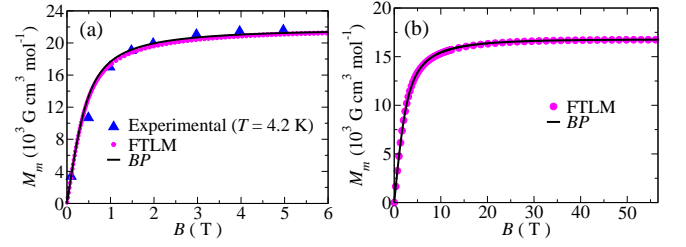


FIG. 3: (Color online) (a) Molar magnetization M_m of the sS chain as a function of B at $T = 4.2$ K. Experimental data of the compound CuMnDTO from Ref. [13]. FTLM results for a chain with $N = 16$, $J/k_B = 44.8$ K and $g = 1.93$. Brillouin paramagnet (BP) with total spin $\bar{S} = 15.0$. (b) FTLM results for M_m of the ssS chain with $N = 18$ as a function of B at $T = 15$ K. BP with $\bar{S} = 8.5$.

note that the FTLM curve for this chain depart from the experimental one at a higher temperature than the curve for the sS chain. This behavior is in fact a finite size effect since the number of unit cells used in the FTLM calculation for the ssS chain (6 unit cells, with 18 sites) is effectively less than the number used for the sS chain (8 unit cells, with 16 sites).

In Fig. 3 we compare our results at $T = 4.2$ K with experimental data from Ref. [13]. The temperature is lower than the one in which the maximum of the χT curve is observed, $T_{max} \approx 7.5$ K. However, due to the low value of the coupling between chains $J_{inter-chain}/k_B \sim 0.1$ K, we expect that at $T = 4.2$ K and for fields higher than ~ 0.1 T, the ferrimagnetic correlations along the chain are the relevant ones to determine the behavior of the magnetization as a function of B . Since the correlation length along the chains diverges [24, 25] as $1/T$, a finite number of unit cells are correlated at 4.2 K. Thus, we can treat the system as composed of independent linear clusters, each cluster carrying a total spin \bar{S} , and a superparamagnetic behavior is expected for the magnetization curve. Within this context, we try to estimate the number of correlated cells in the chain from the experimental data shown in Fig. 3(b) by comparing it with the FTLM data and the molar magnetization of a Brillouin paramagnet (BP) with total spin \bar{S} , given by $M_m(B, T) = N_A g \mu_B (S - s) B_{\bar{S}}(x)$, where N_A is the Avogadro constant and $B_{\bar{S}}(x)$ is the Brillouin function. As shown in Fig. 3(b), the experimental data is well described by the BP curve with $\bar{S} = 15$, indicating that approximately 8 unit cells (size used in the FTLM calculation) are ferrimagnetically correlated at 4.2 K. This enforces the one-dimensional description of the experimental magnetization for this temperature and field values, as well as the superparamagnetic behavior. We remark that the authors of Ref. [13] estimate that approximately 10 cells of the compound CuMnDTO are ferrimagnetically correlated at $T = 7.9$ K (just above T_{max}) for $B = 0$.

For the ssS system, we find no published experimental data for the magnetization. However, considering the

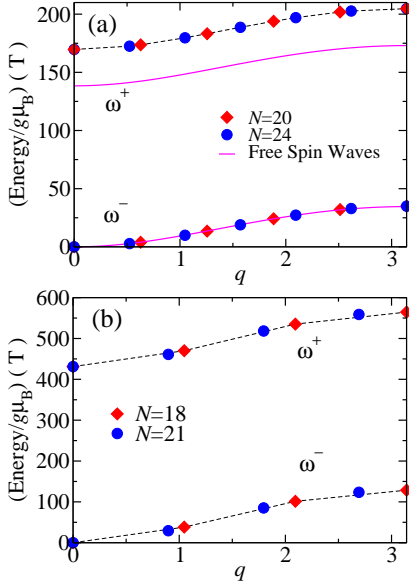


FIG. 4: (Color online) ED results for the lower energy one-magnon bands, in units of magnetic field (using $g = 1.93$), of the (a) sS and (b) ssS chains for the indicated values of N . Full lines are non-interacting spin-wave results from Ref. [26], while dashed lines are guide to the eyes.

FTLM results, Fig. 3(b), we estimate that at $T = 15$ K the number of ferrimagnetically correlated unit cells is ~ 6 (size used in the FTLM calculation), due to the good agreement between the FTLM results and the BP curve with $\bar{S} = 8.75$.

IV. ONE-MAGNON BANDS AND SPECIFIC HEAT

Due to the ferrimagnetic order of the GS, there are two kinds of elementary excitations in the systems: ferromagnetic magnons, which lowers the total spin by one unit and AF magnons, which increases the total spin by one unit. The dispersion relations of the lower energy magnons are calculated, respectively, through

$$\omega^-(q) = E_{\min}(S_{GS} - 1, q) - E_{GS} \quad (4)$$

$$\omega^+(q) = E_{\min}(S_{GS} + 1, q) - E_{GS}, \quad (5)$$

where $E_{\min}(S_t, q)$ indicates the lowest energy in the total-spin sector S_t and lattice wavenumber $q = 2\pi l/N_c$, with $l = 0, 1, 2, \dots, N_c - 1$.

In Figs. 4(a) and 4(b) we display the lower energy one-magnon bands, in units of magnetic field, of the sS and ssS chains. For the sS chain, we also plot in Fig. 4(a) non-interacting spin-wave (SW) results [26]:

$$\omega_{SW}^-(q) = -J(S - s) + \omega_q + g\mu_B B, \quad (6)$$

$$\omega_{SW}^+(q) = J(S - s) + \omega_q - g\mu_B B, \quad (7)$$

where $\omega_q = J\sqrt{(S - s)^2 + 4sS \sin^2(q/2)}$, $s = 1/2$ and

$S = 5/2$. We notice that in zero field the ferromagnetic excitation is gapless (which is expected from the spontaneously broken symmetry of the GS) and display a quadratic dispersion relation in the long wavelength limit, as predicted by conformal invariance [27], while a gap Δ exists for the AF excitation. The ferromagnetic branch obtained through non-interacting SW theory for the sS chain is in good agreement with the ED data, while for the AF branch the value of the zero field gap $\Delta = 2J(S - s) = 4J$ departs from the ED value, as is often the case in other ferrimagnetic systems [28], due to quantum fluctuations effects. In fact, we estimate that in the thermodynamic limit $\Delta = 4.9046J$ ($3.88J$) for the sS (ssS) chain.

In Fig. 5(a) we show the specific heat of the sS and ssS chains in zero field. Due to the LRO ferrimagnetic state at $T = 0 = B$, with low-energy gapless ferromagnetic excitations, it is expected that $C \sim \sqrt{T}$. Another feature is the occurrence of double peaks [29–31]; it turns out that the main peak is well described by the Schottky formula [29, 30]: $\frac{C}{N_c k_B} = \frac{A(\delta/2k_B T)^2}{\cosh^2(\delta/2k_B T)}$, where δ is the Schottky gap and A is the amplitude parameter. The Schottky gap for the ssS chain $\delta_{ssS} \approx 4.1J$ is in accord with the AF spin-wave gap $\Delta_{ssS} \approx 3.9J$. However, for the sS chain the value of $\delta_{sS} (\approx 3.4J)$ significantly departs from the AF spin-wave gap value: $\Delta_{sS} \approx 4.9J$, indicating strong influence of the lower-energy ferromagnetic excitations. Since these states have a total spin ($S_t = S_g - 1$) lower than the one of the AF branch ($S_t = S_g + 1$), we expect that a field B can wash it out. In fact, the center of the AF branch [see Fig. 4(a)] is found at $\bar{\Delta}_{sS}(0) = 5.4J$ and is lowered in the presence of a magnetic field through $\bar{\Delta}_{sS}(B) = \bar{\Delta}_{sS}(0) - g\mu_B B$. In Fig. 5(b) we present the specific heat for fields up to 103.8 T, and in Fig. 5(c) we compare $\bar{\Delta}_{sS}(B)$ with the Schottky gap $\delta_{sS}(B)$. As we can see in the figure, the values of the two quantities are nearly equal for moderate values of B .

V. T - B PHASE DIAGRAM

The GS magnetization per unit cell, m_c , of one-dimensional systems under an applied magnetic field can exhibit plateaus at values such that $S_c - m_c = \text{integer}$, where S_c is the maximum total spin of a unit cell [7]. This condition implies that a plateau can be observed at values of m_c differing from its saturated value by an integer number of spin flips. In particular, a magnetization plateau at $1/3$ of the saturation magnetization was observed in the magnetization curve of the mineral azurite [32], which is generally modeled through the distorted diamond chain [33]. Other compounds exhibiting the $1/3$ magnetization plateau are the trimer chain systems $\text{Cu}_2(\text{P}_2\text{O}_6\text{OH})_2$ [34] and the phosphates [9] $\text{A}_3\text{Cu}_3(\text{PO}_4)_4$, where $A = \text{Ca}, \text{Sr}$ or Pb . Further, the thermal properties of a variety of models [35–37] presenting plateaus in their magnetization curves were analyzed in recent years and it was evidenced that the $1/3$

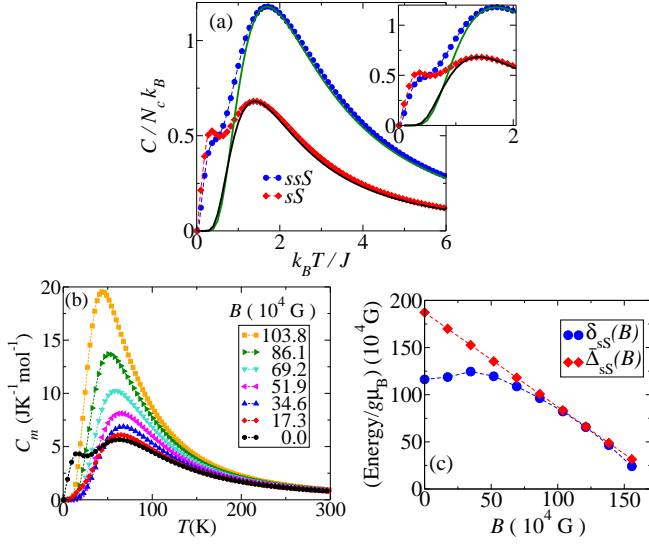


FIG. 5: (Color online) FTLM results. (a) Specific heat of the sS and ssS chains for $B = 0$ as a function of temperature T ; full lines are the respective Schottky specific heats. (b) Molar specific heat C_m of the sS chain for the indicated values of B (using $g = 1.93$); (c) B -dependent Schottky gap $\delta_{ss}(B)$ and spin-wave gap $\Delta_{ss}(B)$. Dashed lines are guide to the eyes.

magnetization plateau is also a characteristic feature of frustrated spin-S chains [38].

For the sS chain studied here, possible plateaus should be observed at $m_c = m_{LM} = g\mu_B(S - s)$ [Lieb-Mattis (LM) magnetization] and $m_c = m_{FP} = g\mu_B(S + s)$ (fully polarized magnetization), as confirmed by the numerical results shown in Fig. 6 (a). In zero field the GS is ferrimagnetic with gapless ferromagnetic excitations [Eq. (6)], while for $B \neq 0$ this mode acquires the gap $\Delta_F(B) = g\mu_B B$. Also, as B increases, the gap for the AF mode [Eq. (7)] decreases linearly with B : $\Delta_{AF}(B) = \Delta_{ss} - g\mu_B B$, and for $g\mu_B B \geq g\mu_B B_m = (\Delta_{ss}/2) \approx 2.45J$ its gap is equal to the ferromagnetic one. At $g\mu_B B = \Delta_{ss} \equiv g\mu_B B_{c,AF}$ the AF gap vanishes and the system undergoes a quantum phase transition (*condensation of AF magnons*, each carrying a spin +1) to a gapless Luttinger Liquid (LL) phase [40], with power-law decay of the transverse correlation functions. In fact, the quantum critical point $B_{c,AF}$ separates an incompressible phase (plateau) from a compressible one (LL phase). For $B \gtrsim B_{c,AF}$, a low-density of magnons is found in the system and the asymptotic singular form of the magnetization can be obtained [41] by considering the system as a free Fermi gas or hard-core bosons. In this limit, the magnons will occupy single particle states with $q \rightarrow 0$ and the dispersion relation, Eq. (7), can be used by replacing the linear spin-wave gap, Δ_{SW} , by the computed gap in Fig. 4(a), $\Delta_{ss} = 4.9046J$:

$$\omega_{AF}^+ = -\mu + \frac{v^2}{2\Delta_{ss}} q^2, \quad q \rightarrow 0, \quad (8)$$

where $v = J\sqrt{2sS} = J\sqrt{5/2}$, $\mu = g\mu_B B - \Delta_{ss} =$

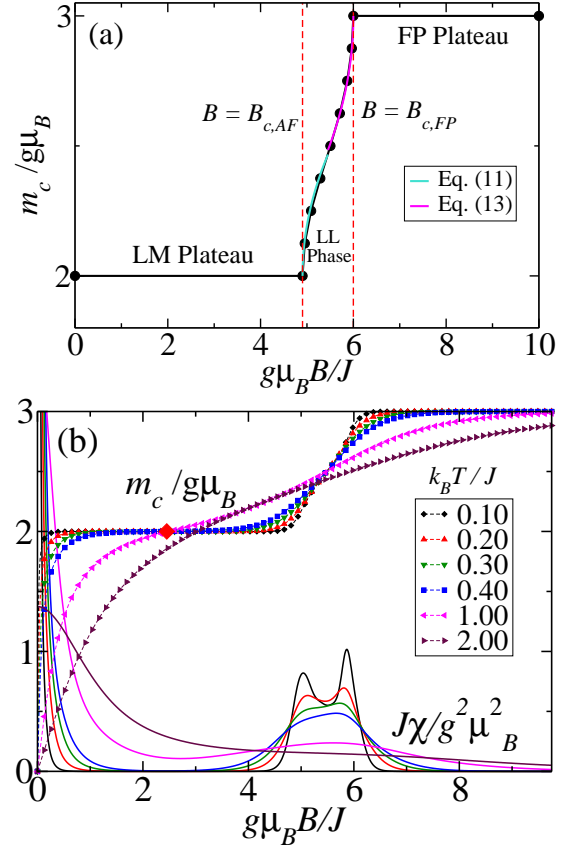


FIG. 6: (Color online) FTLM results for the sS chain. (a) GS magnetization per cell m_c as a function of B for $N = 16$: full circles indicate the midpoints in the steps of the magnetization of the finite-size system and edges of thermodynamic-limit plateaus [39], while colored full lines indicate the results from the free-fermion model (see text). (b) m_c (curves with symbols) and χ (full curves) as a function of B for the listed values of T ; B_m is indicated by the red diamond.

$g\mu_B(B - B_{c,AF})$ and $\Delta_{SW} = 2J(S - s)$. The energy density can thus be written (fermionic map) as

$$\varepsilon = \int_{-k_F}^{k_F} \frac{dk}{2\pi} (\epsilon_k - \mu), \quad (9)$$

where $\epsilon_k = v^2 k^2 / 2\Delta_{ss}$, $k_F = \pi n$, and n is the density of particles. The value of n for a prescribed μ can be obtained from the condition $\partial_n \varepsilon = 0$:

$$n = \sqrt{g\mu_B} \sqrt{\frac{2B_{c,AF}}{\pi^2 v^2}} \sqrt{\mu}, \quad (10)$$

which implies

$$\frac{m_c}{g\mu_B} = 2 + \frac{g\mu_B}{J} \sqrt{\frac{4B_{c,AF}}{5\pi^2}} \sqrt{B - B_{c,AF}}. \quad (11)$$

In Fig. 6(a) we show the very good agreement between the numerical data and m_c given by Eq. (11) in the LL Phase.

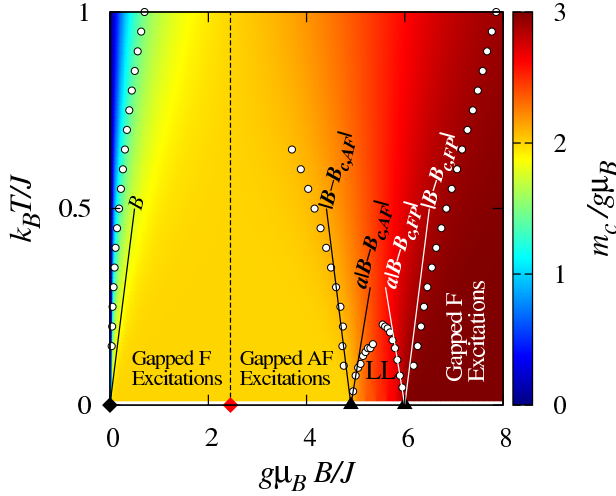


FIG. 7: (Color online) FTLTLM results for the low- T phase diagram of the sS chain: contour plot indicates the magnetization per cell m_c . The critical point at $B = 0$ (black diamond), the inflection point of m_c at $g\mu_B B = g\mu_B B_m = \Delta/2$ (red diamond), the quantum-critical points (black triangles) at $B = B_{c,AF}$ and $B = B_{c,FP}$, crossover lines (white circles) and their asymptotic behavior (full lines) are also indicated.

The gapless LL phase ends at the quantum critical point $B = B_{c,FP}$: the system becomes fully polarized (FP) and presents gapped low energy excitations. The two one-magnon excitations from the FP state, both carrying a spin -1, can be exactly obtained [42] and the lower one has a dispersion relation given by

$$\omega_{FP} = -J(s+S) - J\sqrt{(S-s)^2 + 4sS\cos^2(q/2)} + g\mu_B B, \quad (12)$$

which implies $g\mu_B B_{c,FP} = 2J(s+S) = 6J$, in accord with the numerical results [Fig. 6(a)]. For $B \lesssim B_{c,FP}$, a low density of magnons is observed in the system and the same arguments used to obtain Eq. (10) can be used in this case. For $q \rightarrow 0$, Eq. (12) can be written as Eq. (8) with $v = J\sqrt{2sS} = J\sqrt{5/2}$, $\Delta_F = 2J(s+S) = 6J$ and $\mu = g\mu_B(B_{c,FP} - B)$, which implies, from Eq. (10), that the density of magnons is given by $n = \frac{g\mu_B}{J} \sqrt{\frac{4B_{c,FP}}{5\pi^2}} \sqrt{B_{c,FP} - B}$, and m_c now reads:

$$\frac{m_c}{g\mu_B} = 3 - \frac{g\mu_B}{J} \sqrt{\frac{4B_{c,FP}}{5\pi^2}} \sqrt{B_{c,FP} - B}, \quad (13)$$

which is plotted in Fig. 6(a) and is also in very good agreement with the numerical data.

In Fig. 6(b) we present FTLTLM data for m_c and χ vs. B for $T \neq 0$. We first notice that the magnetization in zero field is null and the system is in the thermal paramagnetic state, as expected from the Mermin-Wagner theorem [22]. Increasing B in the low-temperature regime, the LM (or ferrimagnetic) plateau is exponentially reached and the magnetization exhibits an inflection point at $B = B_m$ [red diamond in Fig. 6(b)] that marks the changing of

the gapped low-energy excitations from ferromagnetic ($B \leq B_m$) to AF magnons ($B \geq B_m$): the ferromagnetic (antiferromagnetic) magnons are exponentially activated and m_c is lower (higher) than $m_{LM} = g\mu_B(S-s)$. Also, by the same token, the FP plateau is exponentially reached from below for fields higher than $B_{c,FP}$. Furthermore, the singular form of the magnetization near the quantum critical points ($B = B_{c,AF}$ and $B = B_{c,FP}$, with $T = 0$), which implies $\chi \rightarrow \infty$, are thermally smoothed out and the singularities in the susceptibility evolve into local maxima, thus providing the determination of the *crossover* lines. The LL phase, with linear dispersion relation $\sim q$, is expected [40] between the two local maxima for a given T [see, e. g., the susceptibility curves for $k_B T = 0.10J$ and $0.20J$ in Fig. 6(b)] with the two local maxima indicating a crossover to a region in which the excitations follow a non-relativistic dispersion relation $\sim q^2$, as previously discussed. On the other hand, as T increases, the LL phase ends and a single maximum is observed in the susceptibility curves (see, e. g., the susceptibility for $k_B T = 0.40J$). This single maximum defines a crossover from the regime in which the physics is determined by the excitations from the LM plateau to a regime in which the FP plateau is the relevant one. For sufficiently high temperatures, the system loses all information about the $T = 0$ LM magnetization plateau and the effect of B is to bring the system from the thermal paramagnetic state to the FP state at higher magnetic fields (see the case $k_B T = 2.00J$).

In Fig. 7 we present the contour plot of m_c in the $T - B$ plane and a schematic phase diagram. The $T - B$ crossover lines enclosing the region of the LL phase, limited at $T = 0$ by $B = B_{c,AF}$ and $B = B_{c,FP}$, are obtained [43] from the local extrema of $m_c(T)$ vs. T for a given B , as shown in Fig. 8(a). Further, as $B \rightarrow B_c$ these crossover lines follow a universal function [43]: $a|B - B_c|$ with $a = 0.76238$; as shown in Fig. 7, our numerical data confirm this asymptotic behavior for the two quantum critical points at $B = B_{c,AF}$ and $B = B_{c,FP}$. Moreover, as T increases beyond the crossover lines of the two plateaus, gapless phases are reached [40, 44]. In addition, by increasing B under a fixed T , local maxima are observed in the specific heat $C(B)$ per spin, as displayed in Fig. 8(b). These features are used to estimate [5] the crossover lines related to the LM plateau and FP plateau shown in Fig. 7; in particular, we notice that $T \sim |B - B_c|$ as the lines reach the corresponding quantum critical points [40, 44]. Last, we stress that the crossover lines and the LL instability lines meet at the quantum critical points, thus delimiting the respective quantum critical region [40, 43–45]; in each region the system is thus governed by the quantum critical point with dynamical exponent $z = 2$ associated with the excited magnons, as discussed above. On the other hand, the magnon densities [40], n , given by $(m_c/g\mu_B) - 2$ and $3 - (m_c/g\mu_B)$ for the quantum critical point at $B = B_{c,AF}$ and $B = B_{c,FP}$, respectively, follow a univer-

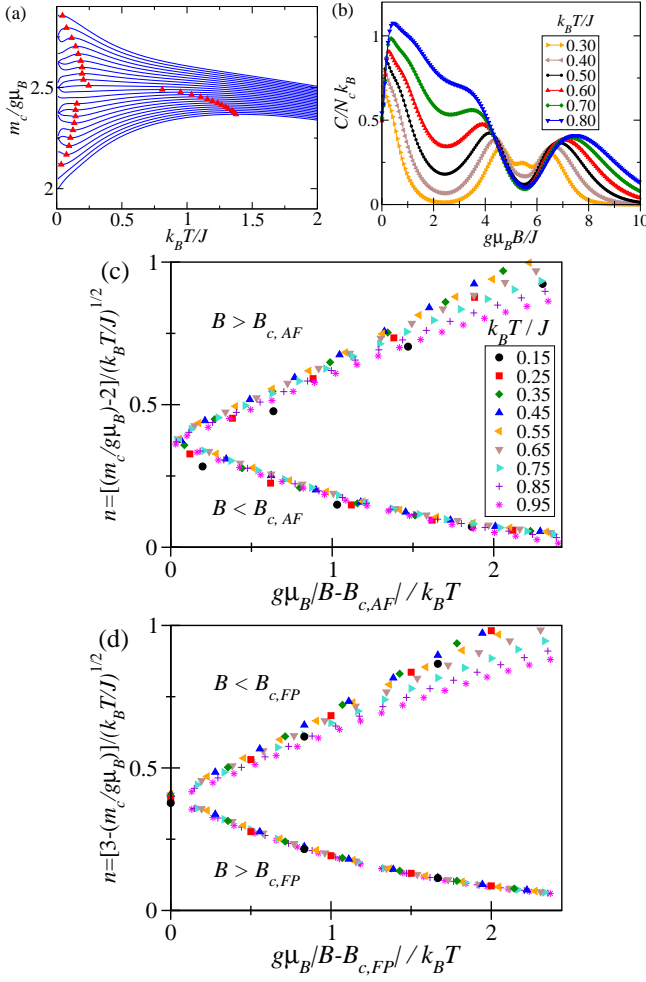


FIG. 8: (Color online) FTLM results for the sS chain. (a) Magnetization per cell m_c as a function of T for fields $g\mu_B B/J$ from 4.85 to 5.95 in steps of 0.05 (from below to top); triangles indicate local maxima associated with the LL crossover lines (see text). (b) Specific heat per cell C as a function of B for the indicated values of temperature. Scaling of the magnon density n around the quantum critical points at (c) $B = B_{c,AF}$ and (d) $B = B_{c,FP}$.

sal function of T and $|B - B_c|/T$:

$$n = \sqrt{\frac{k_B T}{J}} f\left(\frac{|B - B_c|}{T}\right), \quad (14)$$

as shown in Figs. 8 (c) and 8 (d). A better scaling behavior is observed for $B < B_{c,AF}$ ($B > B_{c,FP}$) in Fig. 8 (c) [8 (d)] since for $B > B_{c,AF}$ ($B < B_{c,FP}$) the zone of influence of the quantum critical point at $B = B_{c,FP}$ ($B = B_{c,AF}$) merges with the zone of influence of the point at $B = B_{c,AF}$ ($B = B_{c,FP}$). The guideline $k_B T = g\mu_B B$ in Fig. 7 is discussed below.

In Fig. 9 we present the contour plot of C/T in the $T - B$ phase diagram [5], including the above-discussed crossover lines. At the plateaus, $C/T \rightarrow 0$ as $T \rightarrow 0$ due to the gaps, as evidenced in the plot. As we can

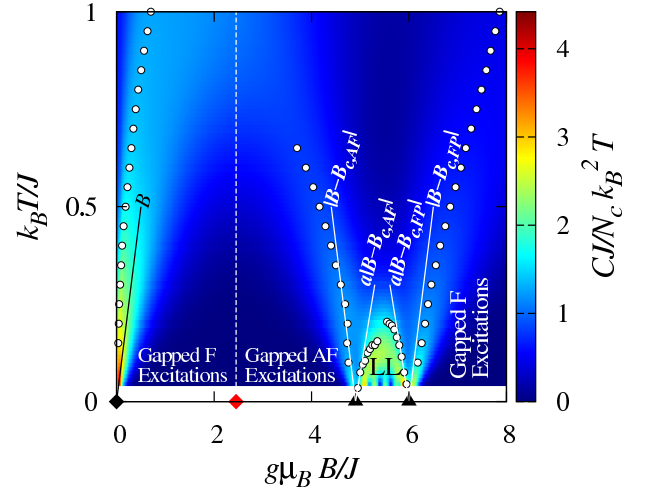


FIG. 9: (Color online) FTLM results for the low- T phase diagram of the sS chain: contour plot indicates C/T . The critical points and crossover lines are indicated as in Fig. 7.

see, the guideline $k_B T = g\mu_B B$ do not coincide with the local maxima of $C(B)$ in the low- B region [see Fig. 8(b)] due to the LRO ferrimagnetic state at $T = 0 = B$: since $C \sim \sqrt{T}$, $C/T \rightarrow \infty$ as $T \rightarrow 0$ at $B = 0$ and an enhancement in the intensity of C/T is observed near $T = 0 = B$. In spite of this fact, the plot shows a depression in the values of C/T near the $T = 0$ LM plateau which, by increasing T , varies in a symmetrical fashion with respect to $B = B_m$ (dome-shaped) and is limited by the $k_B T = g\mu_B B$ and $k_B T = g\mu_B |B_{c,AF} - B|$ asymptotic crossover lines. Further, the LL dome is also clearly seen and the crossover lines of the FP and LM gapped phases can be visualized.

Next, we exhibit in Fig. 10 the magnetization of the ssS chain at $T = 0$. For this chain, the first plateau is found at $m_c = g\mu_B(S - 2s)$, i. e., the LM plateau, and the second is the FP plateau at $m_c = g\mu_B(S + 2s)$; the LL phase is expected to occur between these two plateaus. A third plateau could be found [7] at $m_c = g\mu_B S$; however our numerical shows no evidence of this plateau. We remark that we did not perform a detailed analysis of the $T - B$ phase diagram of this chain, but we expect that it should display similar features already reported for the sS chain.

The huge values of the quantum critical magnetic fields of the CuMnDTO (sS chain) and MnNN (ssS chain) compounds, make the experimental investigation of the full $T - B$ phase diagram of these systems very difficult. However, magnetic phase transitions induced by very large magnetic fields (up to 400 T) in the low-temperature regime have been reported [46]. Further, materials physically described by similar models may have lower values for the exchange coupling and thus a more experimentally accessible phase diagram.

We also mention that ferrimagnetism can be destabilized by competing (or frustrating) interactions [47, 48],

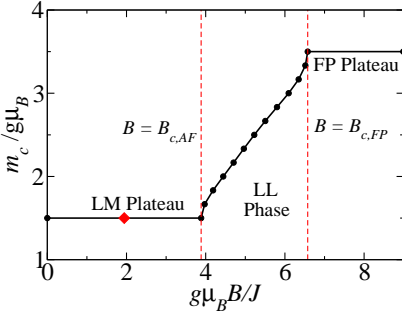


FIG. 10: (Color online) FTLM results for the magnetization per cell m_c of the ssS chain as a function of field B at $T = 0$ for $N = 18$. Full circles indicate the midpoints in the steps of the magnetization of the finite-size system and edges of thermodynamic-limit plateaus [39].

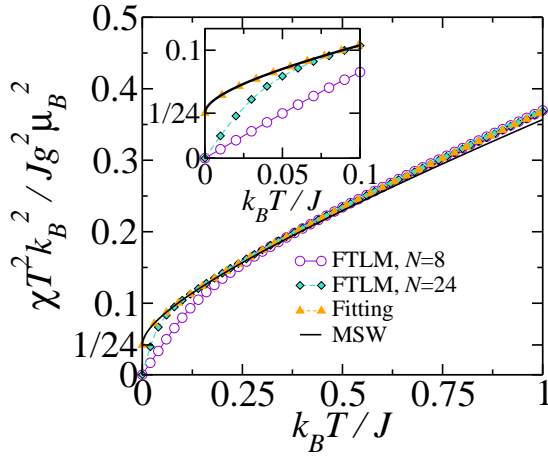


FIG. 11: (Color online) χT^2 vs. T for the spin-1/2 ferromagnetic chain in the low and very low ($k_B T \ll J$) temperature regions. FTLM results for $N = 8$ and $N = 24$. Fitting of the FTLM results for $N = 8$ using $[\frac{1}{24} + a_0(\frac{k_B T}{J})^{\frac{1}{2}} + a_1(\frac{k_B T}{J})]$ (see text). MSW results up to second order in $k_B T/J$. The inset shows the results for $k_B T \leq 0.1J$.

which can give rise to other critical points. Unconventional ferrimagnetism (non-bipartite lattices) was indeed found in one-dimensional frustrated structures [49, 50] and in the Kagomé lattice [51]. Further, the magnetocaloric effect in the kinetically frustrated diamond chain was recently investigated [52].

VI. LOW-TEMPERATURE MAGNETIC SUSCEPTIBILITY

We now consider the temperature regime where ferromagnetic excitations tend to be a predominant feature. In order to test and illustrate the accuracy of the FTLM in describing the susceptibility behavior at very low temperatures, we have calculated the susceptibility of the spin-1/2 linear *ferromagnetic* chain; the results for χT^2

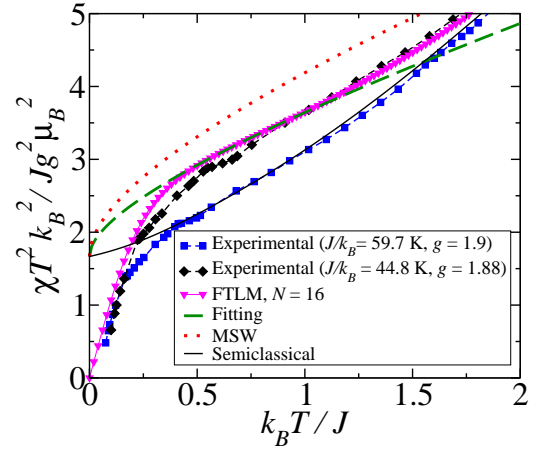


FIG. 12: (Color online) χT^2 vs. T for the sS chain. Experimental data of the compound CuMnDTo from Ref. [13]. FTLM results for $N = 16$. Fitting of the FTLM results for $N = 16$ using $[\frac{5}{3} + a_0(\frac{k_B T}{J})^{\frac{1}{2}} + a_1(\frac{k_B T}{J})]$ (see text). MSW results up to second order in $k_B T/J$ from Ref. [29]. The semiclassical results are from Ref. [19].

as a function of T are shown in Fig. 11 for systems with 8 and 24 sites. The crossover to zero of the FTLM results as $T \rightarrow 0$ is due to finite size effects. We note that for $(k_B T/J) \gtrsim 0.3$ the curves for the two chain sizes superimpose, thus suggesting that the thermodynamic-limit behavior has already been within numerical accuracy. Also, in the temperature range $0.06 \lesssim (k_B T/J) \approx 0.1$, the results for the larger system is in good agreement with the expansion formula from Takahashi's MSW theory [23], which up to second order in $t \equiv k_B T/J$ reads: $\frac{\chi J}{(g\mu_B)^2} = t^{-2} \left[\frac{2}{3}s^4 - 2\frac{1}{2}s^{\frac{5}{2}}At^{\frac{1}{2}} + sA^2t + O(t^{\frac{3}{2}}) \right]$, where $A = \zeta(\frac{1}{2})/\sqrt{2\pi} \approx -0.582597$ and $g = 2$. For $s = 1/2$ we obtain

$$\frac{\chi J}{(g\mu_B)^2} = t^{-2} \left[\frac{1}{24} + 0.145649t^{\frac{1}{2}} + 0.16971t + O(t^{\frac{3}{2}}) \right] \quad (15)$$

We stress that in the range $0 < (k_B T/J) < 0.1$, Eq. (15) is in very good agreement with predictions from the Bethe-ansatz approach [53], while the fitting of the FTLM results for $N = 8$ and $0.5 < (k_B T/J) < 0.9$, yields $a_0 = 0.140$ and $a_1 = 0.186$, in good agreement with the MSW coefficients.

We now turn our attention to the low-temperature regime of the sS-chain susceptibility displayed in Fig. 12. Firstly, we note that for $(k_B T/J) \gtrsim 0.5$ the FTLM results for $N = 14$ (not shown) and $N = 16$ (8 cells) coincide, indicating that the thermodynamic limit has been attained in this temperature range. The experimental data normalized by $J/k_B = 44.8$ K ($g = 1.88$) and $J/k_B = 59.7$ K ($g = 1.9$) show the expected agreement with the FTLM results and the semiclassical formula, respectively, as already displayed in Fig. 2(a). The MSW results comes from the expansion formula derived by Yamamoto *et al.*

[29], which up to second order in t reads:

$$\frac{\chi J}{(g\mu_B)^2} = t^{-2} \left[\frac{Ss(S-s)^2}{3} - (Ss)^{\frac{1}{2}}(S-s)^{\frac{3}{2}}At^{\frac{1}{2}} + (S-s)A^2t + O\left(t^{\frac{3}{2}}\right) \right]. \quad (16)$$

A relevant aspect of this expansion is that for $S = 2s$ we recover the Takahashi expansion for the ferromagnetic linear chain of spin s , which reinforces that the ferromagnetic excitation is the relevant one at low temperatures [29]. Setting $s = 1/2$ and $S = 5/2$ in Eq. 16, we obtain

$$\frac{\chi J}{(g\mu_B)^2} = t^{-2} \left[\frac{5}{3} + 1.842334t^{\frac{1}{2}} + 0.678840t + O\left(t^{\frac{3}{2}}\right) \right], \quad (17)$$

The FTLM results can be fitted by a function of the form $[\frac{5}{3} + a_0(\frac{k_B T}{J})^{\frac{1}{2}} + a_1(\frac{k_B T}{J})]$. Guided by our studies on the spin-1/2 ferromagnetic chain, we have chosen the interval $0.5 \leq (k_B T/J) \leq 0.9$ to fix the values of a_0 and a_1 : $a_0 = 1.28$ and $a_1 = 0.69$, which can be compared with those in Eq. (17), and implies a good agreement for the integer-power coefficient and an order-of-magnitude agreement for the half-integer power coefficient.

One should notice that the FTLM results and the experimental data crossover to zero as $(k_B T/J) \rightarrow 0$, instead of approaching the constant value $sS(S-s)^2/3 = 5/3$. Here one must distinguish two effects: with respect to FTLM, this is evidently a manifestation of finite-size effects, while for the experimental data one can attribute this to the 1D/3D crossover that takes place below $T = 7.5$ K (see Sec. III). In fact, in the 3D region the susceptibility behaves as $\chi \sim T^{-\gamma}$, with the critical exponent $\gamma < 2$, implying that $\chi T^2 \rightarrow 0$ as $T \rightarrow 0$.

VII. SUMMARY AND DISCUSSION

We have presented a thorough numerical study of the GS and thermodynamic properties of two one-

dimensional models related to quasi-one-dimensional ferrimagnetic compounds: CuMnDTO and MnNN. In fact, the models are associated to two types of ferrimagnetic chains: the alternating spin-1/2 spin-5/2 chain and the spin-1/2 spin-5/2 alternating chain with a spin-1/2 pendant attached to the spin-5/2 site. The finite temperature Lanczos method proved quite reliable, except at very low temperatures where finite-size effects hinder its accuracy. A particular feature of these systems is the presence of gapless ferromagnetic and gapped AF spin-wave (magnon) branches in zero field. As the magnetic field is increased, the low-energy excitation changes from ferromagnetic to AF and the magnetic field vs. temperature phase diagram displays characteristic crossover lines which distinguish these systems from spin-1 Haldane chains and two-leg ladder models. In particular, for the sS chain we have identified the quantum critical points and the crossover lines, the Luttinger liquid phase, the ferrimagnetic (LM) and the fully polarized plateaus. The values of the exchange coupling parameters of the compounds discussed in the text are indeed very high. However, magnetic phase transitions induced by very large magnetic fields (up to 400 T) in the low-temperature regime have been experimentally investigated[46]. Also, other compounds described by similar models can have lower values of the exchange parameters and a more experimentally accessible phase diagram. We expect that this work stimulates experimental and theoretical research with focus on the phase transitions induced by an applied magnetic field in the low-temperature regime of the large class of quasi-one-dimensional ferrimagnetic compounds.

VIII. ACKNOWLEDGMENTS

This work was supported by CNPq, FACEPE, CAPES, and Finep (Brazilian agencies).

-
- [1] T. Giamarchi, *Quantum physics in one dimension* (Oxford University Press, USA, 2004).
 - [2] N. B. Ivanov, J. Schnack, R. Schnalle, J. Richter, P. Kögerler, G. N. Newton, L. Cronin, Y. Oshima, and H. Nojiri, *Phys. Rev. Lett.* **105**, 037206 (2010).
 - [3] M. Takahashi, *Thermodynamics of one-dimensional solvable models* (Cambridge Univ Pr, 1999).
 - [4] S. Sachdev, *Quantum Phase Transitions* (Cambridge University Press, Cambridge, UK, 1999); M. Vojta, *Rep. Prog. Phys.* **66**, 2069 (2003); S. Sachdev and B. Keimer, *Phys. Today* **64**, 29 (2011).
 - [5] C. Rüegg, K. Kiefer, B. Thielemann, D. F. McMorrow, V. Zapf, B. Normand, M. B. Zvonarev, P. Bouillot, C. Kollath, T. Giamarchi, S. Capponi, D. Poilblanc, D. Biner, and K. W. Krämer, *Phys. Rev. Lett.* **101**, 247202 (2008).
 - [6] P. Bouillot, C. Kollath, A. M. Läuchli, M. Zvonarev, B. Thielemann, C. Rüegg, E. Orignac, R. Citro, M. Klanjšek, C. Berthier, M. Horvatić, and T. Giamarchi, *Phys. Rev. B* **83**, 054407 (2011).
 - [7] M. Oshikawa, M. Yamanaka, and I. Affleck, *Phys. Rev. Lett.* **78**, 1984 (1997).
 - [8] A. M. S. Macêdo, M. C. dos Santos, M. D. Coutinho-Filho, and C. A. Macêdo, *Phys. Rev. Lett.* **74**, 1851 (1995).
 - [9] M. Matsuda, K. Kakurai, A. A. Belik, M. Azuma, M. Takano, and M. Fujita, *Phys. Rev. B* **71**, 144411 (2005); A. A. Belik, A. Matsuo, M. Azuma, K. Kindo, and M. Takano, *J. Solid State Chem.* **178**, 709 (2005) and references therein.
 - [10] M. Drillon, M. Belaiche, P. Legoll, J. Aride, A. Boukhari,

- and A. Moqine, J. Magn. Magn. Mater. **128**, 83 (1993).
- [11] S. Yamamoto and J. Ohara, Phys. Rev. B **76**, 014409 (2007).
- [12] A. Gleizes and M. Verdaguer, J. Am. Chem. Soc. **103**, 7373 (1981).
- [13] M. Verdaguer, A. Gleizes, J.-P. Renard, and J. Seiden, Phys. Rev. B **29**, 5144 (1984).
- [14] A. Caneschi, D. Gatteschi, and R. Sessoli, Inorg. Chem. **32**, 4612 (1993) and references therein.
- [15] K. Fegy, D. Luneau, E. Belorizky, M. Novac, J.-L. Tholence, C. Paulsen, T. Ohm, and P. Rey, Inorg. Chem. **37**, 4524 (1998).
- [16] Y. Pei, M. Verdaguer, O. Kahn, J. Sletten, and J.-P. Renard, Inorg. Chem. **26**, 138 (1987).
- [17] E. Lhotel, V. Simonet, E. Ressouche, B. Canals, D. B. Amabilino, C. Sporer, D. Luneau, J. Veciana, and C. Paulsen, Phys. Rev. B **75**, 104429 (2007); E. Lhotel, D. B. Amabilino, C. Sporer, D. Luneau, J. Veciana, and C. Paulsen, Phys. Rev. B **77**, 064416 (2008).
- [18] J. Jaklič and P. Prelovšek, Adv. Phys. **49**, 1 (2000).
- [19] J. Seiden, J. Phys. **44**, L947 (1983).
- [20] E. H. Lieb and D. Mattis, J. Math. Phys. **3**, 749 (1962).
- [21] M. Drillon, E. Coronado, R. Georges, J. C. Gianduzzo, and J. Curely, Phys. Rev. B **40**, 10992 (1989).
- [22] N. D. Mermin and H. Wagner, Phys. Rev. Lett. **17**, 1133 (1966).
- [23] M. Takahashi, Phys. Rev. Lett. **58**, 168 (1987).
- [24] E. P. Raposo and M. D. Coutinho-Filho, Phys. Rev. Lett. **78**, 4853 (1997); E. P. Raposo and M. D. Coutinho-Filho, Phys. Rev. B **59**, 14384 (1999).
- [25] C. Vitoriano, M. D. Coutinho-Filho, and E. P. Raposo, J. Phys. A: Math. Gen. **35**, 9049 (2002).
- [26] S. Pati, S. Ramasesha, and D. Sen, Phys. Rev. B **55**, 8894 (1997); S. Brehmer, H.-J. Mikeska, S. Yamamoto, J. Phys. Condens. Matter **9**, 3921 (1997).
- [27] F. C. Alcaraz and A. L. Malvezzi, J. Phys. A: Math. and Gen. **30**, 767 (1997).
- [28] R. R. Montenegro-Filho and M. D. Coutinho-Filho, Physica A **357**, 173 (2005); S. Yamamoto and J. Ohara, Phys. Rev. B **76**, 014409 (2007).
- [29] S. Yamamoto and T. Fukui, Phys. Rev. B **57**, R14008 (1998). Spin-wave interaction effects were analyzed by S. Yamamoto, T. Fukui, K. Maisinger, and U. Schollwöck, J. Phys.: Condens. Matter **10**, 11033 (1998), and S. Yamamoto, Phys. Rev. B **69**, 064426 (2004).
- [30] T. Nakanishi and S. Yamamoto, Phys. Rev. B **65**, 214418 (2002).
- [31] R. Pelka and D. Pinkowicz, Acta Phys. Polon. A **118**, 959 (2010).
- [32] H. Kikuchi, Y. Fujii, M. Chiba, S. Mitsudo, T. Idehara, T. Tonegawa, K. Okamoto, T. Sakai, T. Kuwai, and H. Ohta, Phys. Rev. Lett. **94**, 227201 (2005); K. C. Rule, A. U. B. Wolter, S. Süllow, D. A. Tennant, A. Brühl, S. Köhler, B. Wolf, M. Lang, and J. Schreuer, Phys. Rev. Lett. **100**, 117202 (2008); F. Aimò, S. Krämer, M. Klanjšek, M. Horvatić, C. Berthier, and H. Kikuchi, Phys. Rev. Lett. **102**, 127205 (2009).
- [33] K. Okamoto, T. Tonegawa, and M. Kaburagi, J. Phys.: Condens. Matter **15**, 5979 (2003); B. Gu and G. Su, Phys. Rev. B **75**, 174437 (2007); K. Hida, K. Takano, and H. Suzuki, J. Phys. Soc. Jpn. **78**, 084716 (2009).
- [34] M. Hase, M. Kohno, H. Kitazawa, N. Tsujii, O. Suzuki, K. Ozawa, G. Kido, M. Imai, X. Hu, Phys. Rev. B **73**, 104419 (2006).
- [35] S.-S. Gong, W. Li, Y. Zhao, and G. Su, Phys. Rev. B **81**, 214431 (2010).
- [36] S.-S. Gong, S. Gao, and G. Su, Phys. Rev. B **80**, 014413 (2009).
- [37] B. Gu, G. Su, and S. Gao, Phys. Rev. B **73**, 134427 (2006).
- [38] F. Heidrich-Meisner, I. A. Sergienko, A. E. Feiguin, and E. R. Dagotto, Phys. Rev. B **75**, 064413 (2007).
- [39] J. C. Bonner and M. E. Fisher, Phys. Rev. **135**, A640 (1964).
- [40] R. Chitra and T. Giamarchi, Phys. Rev. B **55**, 5816 (1997).
- [41] A. M. Tsvelik, Phys. Rev. B **42**, 10499 (1990); I. Affleck, Phys. Rev. B **43**, 3215 (1991); E. S. Sørensen and I. Affleck, Phys. Rev. Lett. **71**, 1633 (1993).
- [42] S. Yamamoto and H. Hori, Phys. Rev. B **72**, 054423 (2005).
- [43] Y. Maeda, C. Hotta, and M. Oshikawa, Phys. Rev. Lett. **99**, 057205 (2007).
- [44] S. Sachdev, T. Senthil, and R. Shankar, Phys. Rev. B **50**, 258 (1994).
- [45] G. Chaboussant, M.-H. Julien, Y. Fagot-Revurat, M. Hanson, L. P. Lévy, C. Berthier, M. Horvatić, and O. Piovesana, Eur. Phys. J. B **6**, 167 (1998).
- [46] E. Kojima, A. Miyata, S. Miyabe, S. Takeyama, H. Ueda, and Y. Ueda, Phys. Rev. B **77**, 212408 (2008); E. Kojima, A. Miyata, Y. Motome, H. Ueda, Y. Ueda and S. Takeyama, J. Low Temp. Phys. **159**, 3 (2010); A. Miyata, E. Kojima, H. Ueda, Y. Ueda, Y. Motome, S. Takeyama J. Phys. Conf. Ser. **200**, 032046 (2010).
- [47] N. B. Ivanov, Condens. Matter Phys. **12**, 435 (2009).
- [48] V. R. Chandra, N. B. Ivanov, and J. Richter, Phys. Rev. B **81**, 024409 (2010).
- [49] R. R. Montenegro-Filho and M. D. Coutinho-Filho, Phys. Rev. B **78**, 014418 (2008); A. S. F. Tenório, R. R. Montenegro-Filho, and M. D. Coutinho-Filho, Phys. Rev. B **80**, 054409 (2009).
- [50] T. Shimokawa and H. Nakano, J. Phys. Soc. Jpn. **80**, 043703 (2011).
- [51] K. Hida, K. Takano, and H. Suzuki, J. Phys. Soc. Jpn. **78**, 033709 (2009).
- [52] M. S. S. Pereira, F. A. B. F. de Moura, and M. Lyra, Phys. Rev. B **79**, 054427 (2009).
- [53] M. Takahashi, Prog. Theor. Phys. **46**, 401 (1971).